Deterministic switching of the growth direction of self-catalyzed GaAs nanowires

*Eero S. Koivusalo** [1]*, Teemu V. Hakkarainen*[1]*, Helder V. A. Galeti*[2]*, Yara G. Gobato*[3]*, Vladimir G. Dubrovskii*[4]*, Mircea D. Guina*[1]

[1] Optoelectronics Research Centre, Tampere University of Technology, P.O. Box 692, FIN-33101 Tampere

[2] Electrical Engineering Department, Federal University of São Carlos, 13565-905, São Carlos-SP, Brazil

[3] Physics Department, Federal University of São Carlos, 13565-905, São Carlos-SP, Brazil

[4] ITMO University, Kronverkskiy prospekt 49, 197101 St. Petersburg, Russia

ABSTRACT: Typical vapor-liquid-solid growth of nanowires is restricted to vertical one-dimensional geometry, while there is a broad interest for more complex structures in the context of electronics and photonics applications. Controllable switching of the nanowire growth direction opens up new horizons in the bottom-up engineering of self-assembled nanostructures, for example, to fabricate interconnected nanowires used for quantum transport measurements. In this work, we demonstrate a robust and highly controllable method for deterministic switching of the growth direction of self-catalyzed GaAs nanowires. The method is based on the modification of the droplet-nanowire interface in the annealing stage without any fluxes and subsequent growth in the horizontal direction by a twin-mediated mechanism with indications of a novel type of interface oscillations. A 100% yield of switching the nanowire growth direction from vertical to horizontal is achieved by systematically optimizing the growth parameters. A kinetic model describing the competition of different interface structures is introduced to explain the switching mechanism and the related nanowire geometries. The model also predicts that growth of similar structures is possible for all vapor-liquid-solid nanowires with commonly observed truncated facets at the growth interface.

KEYWORDS Self-catalyzed GaAs nanowires, Growth direction, Crystal facets, Surface energetics

Precise shaping of III-V semiconductor nanowires (NWs) is paramount for their functionalization into electronic and photonic devices. In particular, GaAs/AlGaAs NW-based lasers integrated on silicon waveguides [1], monolithic LEDs [2, 3], and functional NW array solar cells [4] have been the important milestones in this development. All–these achievements have relied on the axial or radial heterostructures within one-dimensional (1D) NWs. Extension of the NW growth beyond 1D geometry provides a suitable template for delicate quantum transport measurements [5, 6]. Several approaches have previously been used to form a versatility of three-dimensional NW-based structures. In particular, Au-catalyzed NW crosses have been grown on a (100) substrate producing rather random InAs NW meshes [6], and in a more controllable way on a pre-patterned substrate [7]. A ridged template covered by oxide with pre-determined nucleation sites has provided another approach to grow more regular InAs [8, 9] and InSb [5] NW crosses. Interconnected NWs can also be produced by switching the NW growth direction with respect to the typical <111> [or <0001> in the case of wurtzite (WZ) NWs] direction of the substrate normal. The most convenient 90° switching of the growth direction has been demonstrated for Au-catalyzed WZ InAs NWs [7] and catalyst-free InAs(Sb) NWs [10]. In optics and photonics, possible applications of such structures include circular dichroism in the optical response of chiral nanostructures [11], exploiting the waveguiding properties of semiconductor NWs. [12, 13] This effect further increases the interest in controlling the NW growth direction. To date, the yield of bent NWs has always been less than 100 % within the framework of self-catalyzed approach. Furthermore, not all the horizontal growths start in the same horizontal plane, which is unfavorable for further contacting the NWs.

The simplest mechanism for switching the NW growth direction is driven by a catalyst droplet wetting one of the NW side facets [7, 10, 14]. After that, more complex growth effects may occur, including the formation of new facets or twin planes separating different facets. Using these effects, even reversible switching of the growth direction has been demonstrated in Au-catalyzed InP NWs [15]. In addition, twinning is known to facilitate the formation of kinks and other kind of structures such as nanomembranes [16], flags [14] and sails [17]. Very important information on the kinetics of kinking in Au-catalyzed NWs is provided by in-situ transmission electron microscopy (TEM), as descried previously [18, 19]. Despite the significant progress in understanding and controlling the NW growth direction by different methods, a simple and robust procedure for achieving 100% yield of horizontal self-catalyzed NW growth in one horizontal plane is still lacking. Consequently, this work reports a method to grow very regular ensembles of 90° bent GaAs NWs on silicon in the self-catalyzed approach.

By using a lithography-free SiO_x patterns as templates for the self-catalyzed vapor-liquid-solid (VLS) growth, we have been able to obtain GaAs NWs with the controllable number density, high quality zincblende (ZB) crystal structure and remarkable sub-Poissonian length uniformity [20–22]. Here, we show that this growth method can be extremely suitable to induce bent NW structures with horizontal growth. The deterministic switching of the growth direction occurs in the same horizontal plane due to the narrow length distribution of the initial NWs. This is highly desirable for fabrication of interconnected NWs. 100% yield of regularly bent NWs is achieved simply by a growth interruption, which determines a transition from vertical to horizontal growth. We investigate in detail the previously unknown growth mechanism in different stages and show that the NW morphology is generally sensitive to the duration of the growth interruption, the local V/III ratio, and the NW diameter. Longer growth interruption is found to deterministically switch the NW growth direction by 90° with a 100% yield. We develop a model, which describes the observed reshaping of the growth interface and shows that the deterministic transition from vertical to horizontal growth upon the growth interrupt must be a general phenomenon for all self-catalyzed III-V NWs under the appropriate conditions. Thus, the insights presented here may help to either avoid the unwanted kinking during the NW growth or deterministically switch the NW growth direction when required for particular applications.

The self-catalyzed GaAs NWs were grown by solid source molecular beam epitaxy (MBE) on lithography-free oxide pattern templates fabricated on p-Si(111) substrates via droplet epitaxy. The lithography-free templates are fabricated on HF etched, oxide-free Si substrates, by depositing Ga droplets on the substrate and crystallizing the droplets into GaAs under the As flux. After that, the templates are oxidized in air and loaded back into the MBE chamber, where the GaAs mounds are evaporated to form the lithography-free oxide patterns, on which the NWs are *in-situ* grown, as described in [20, 22]. The NWs were grown on four different templates with the nucleation site densities varying from 5×10^{7} cm^{-2} to 5×10^{8} cm^{-2}. The vertical NW growth was initiated with a 40 s pre-deposition of Ga droplets, re-evaporation of the droplets and simultaneously opening the Ga and As_2 fluxes. The NW growth was conducted at 640 °C, as determined by pyrometer, the Ga deposition rate was 0.3 μm/h, as calibrated for (100) GaAs growth, and the V/III beam equivalent pressure (BEP) ratio was 9. The vertical NW growth time was 20 min, except for three samples with variable diameters for which the growth durations from 20 to 30 min were used. More details on the template fabrication and the NW growth method can be found in Refs. [20–22]. After growth of the vertical part, the NWs were annealed for 20 to 70 s at the growth temperature without any fluxes in order to reshape the droplet-NW interface. After the annealing, the NW growth was resumed by simultaneously providing the Ga and As fluxes. The V/III BEP ratio for the horizontal growth was varied from 7 to 11. After growth, the samples were rapidly cooled down. Additional samples with vertical NWs grown for 20 min and rapidly cooled down (template density 5×10^{8} cm^{-2}), and NWs gone through 45 s annealing (template densities 2×10^{8} cm^{-2}, 5×10^{8} cm^{-2} and 5×10^{7} cm^{-2}, and growth durations from 20 to 30 min) were also fabricated as the references to study the droplet-NW interface and the NW dimensions before the growth continuation.

The NW morphologies were studied using scanning electron microscopy (SEM). A typical NW sample after 20 min of vertical growth and immediate cool down without any fluxes is shown in Figures 1 (a) and (d). It is clearly seen that the Ga droplets remain stationary on the NW tips just after growth. In contrast, the sample that was annealed for 45 s at the growth temperature prior to cool down [Figure 1 (b) and (e)] exhibits 100% yield of droplets falling toward one of the (110) side facets. When the growth is resumed after annealing by simultaneously opening the Ga shutter and As valve, the NWs continue their growth perpendicular to their initial growth direction [Figures 1 (c) and (f)], or slightly downward [Figures 1 (c) and (g)]. Perpendicularly grown horizontal sections are referred to as type 1 and downward pointing sections as type 2. The azimuthal direction of the bent NW part is toward one of the <112> directions associated with the corners of the (110) sidewalls, in contrast to the droplet position after the annealing [see the top-view images in Figures 1 (e) to (g)].

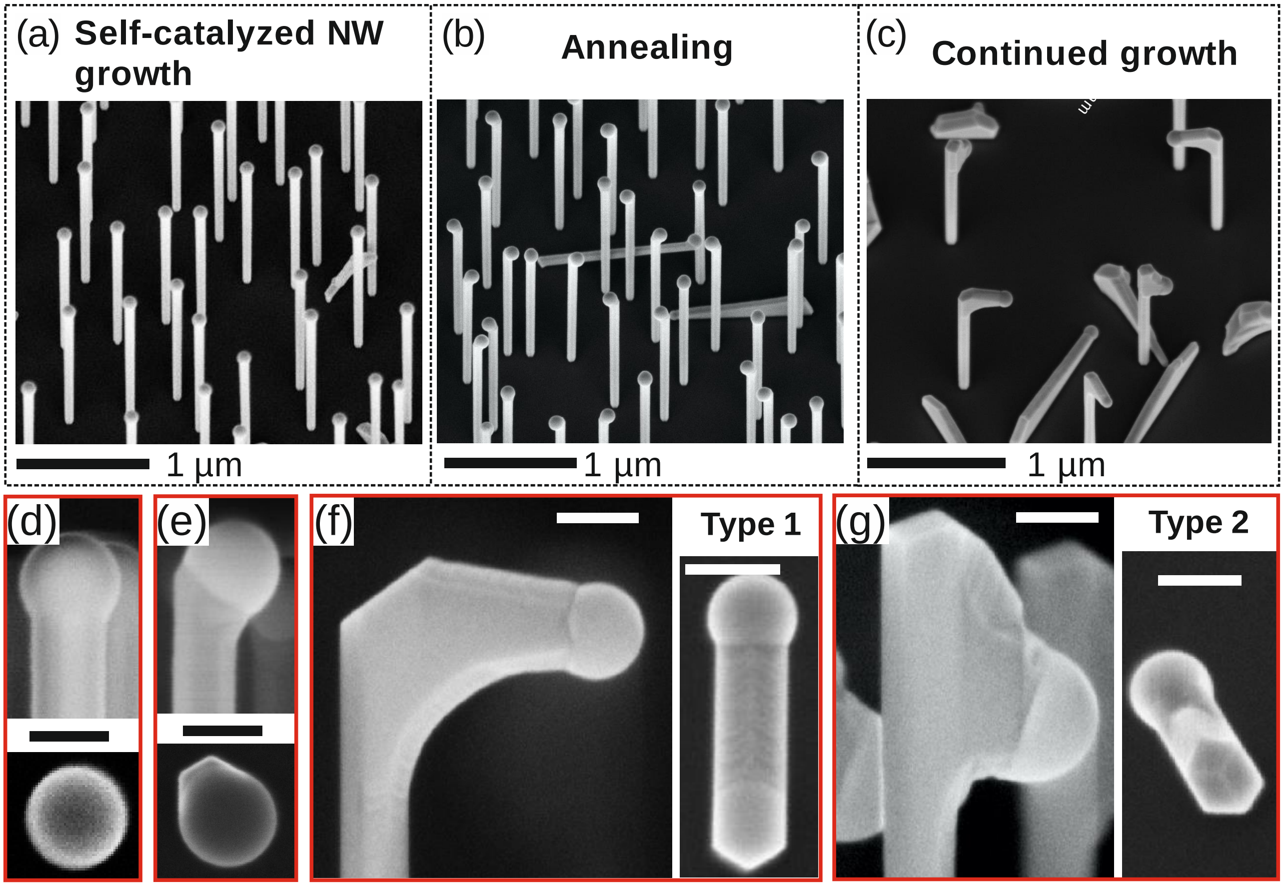

Figure 1. Growth of bent GaAs NWs: (a) and (d) Vertical NWs grown for 20 min and rapidly cooled down; (b) and (e) NWs annealed at the growth temperature for 45 s prior to cool down; (c) NWs grown for 5 min after 45 s annealing; Side- and top-view images of (f) type 1 horizontal and (g) type 2 downward growth. Scale bars in low magnification 30° tilted images are 1 µm in (a) to (c) and 100 nm in (d) to (g).

To further understand the formation mechanism of these structures, the post-annealing droplet-NW interfaces were analyzed by SEM and high-resolution transmission electron microscopy (HR-TEM) [JEOL JEM-2200FS operated at 200 kV and FEI Tecnai G2-F20 operated at 200 kV for Figure 4 (b)]. Two different droplet–NW interface shapes with respect to the [110] zone axis (ZA) were found by TEM, as shown in Figures 2 (a) and (b). The first shape is dominated by the A-polar (1-1-1) facet and the second type by the (0-10) facet. The third low index facet is the B-polar (-111) facet forming below the (0-10) one, as shown in Figure 2(b). Otherwise, the structures compose of minor higher index facets. The facets are identified based on the assumption that the NW top facet is (-1-1-1) and the NW sidewalls are (110). The growth direction is identified as <111>B because it is the common growth direction of self-catalyzed GaAs NWs [23, 24], while A-polar GaAs NWs are rarely achieved and mainly using Au-catalyzed VLS growth [25, 26]. It should also be noted that the radial symmetry of the NW is three-fold. This symmetry yields three possible sets of [110] ZA that give equivalent results for the facet identification. The one presented here is an arbitrarily chosen example showing the droplet-NW interface of a particular NW.

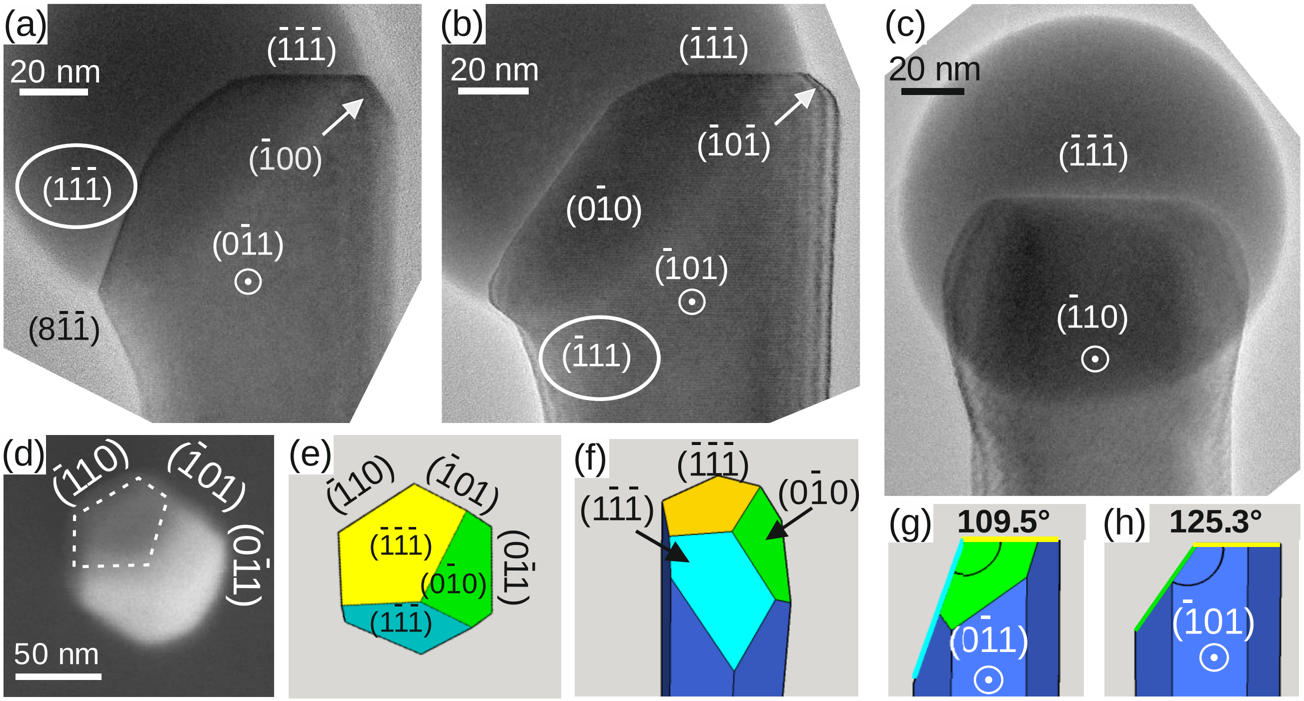

Figure 2. (a)–(c) TEM micrographs of three NWs annealed for 45 s at the growth temperature prior to cool down. The ZAs marked in the micrographs are also marked in the SEM image of droplet-free NW top facet in (d) and sketches (e), (g) and (h). SEM image (d) and top-view sketch (e) are aligned with respect to each other. Complementary SEM analysis of (d) is presented in the SI.

Both dominating reshaped facets are inclined toward one of the <112> corner directions of the NW sidewalls, perpendicular to the [110] ZA used for imaging. However, back-view TEM [Figure 2 (c)] and top-view SEM [Figure 1 (e)] show that the droplets are tilted symmetrically toward one of the (110) side facets. The shape of the NW growth interface was imaged by SEM after removing the Ga droplets by HCl etching. SEM analysis revealed the pentagonal shape of the top facet marked by the dashed line in Figure 2 (d), and that two of the sidewall corners are hidden under the reshaped facets. Based on these results, the interface configurations shown in Figures 2 (a) and (b) are interpreted as different views of similar structure, illustrated in the sketches in Figures 2 (e)–(h). More details on the SEM analysis of the droplet-NW interface are given in the supporting information (SI).

Results of the TEM analysis of a type 1 NW structure, shown in Figures 3 (a) and (b), reveal pure ZB structure throughout the whole NW, with a single twin plane extending along the horizontal section HR-TEM images in Figures 3 (c) to (e) are aligned in such a way that the top side of the horizontal section is facing upward. These images show two different interface configurations existing during growth of type 1 horizontal sections. Both configurations are dominated by a flat (111) plane on one side of the twin plane, and feature a combination of smaller facets on the other. For the NW imaged in Figure 3 (c), the dominating flat (111) plane is B-polar as it is situated above the twin plane. For the NW in Figure 3 (d), the dominating (111) plane is A-polar, and lies below the twin plane. This (111) A facet corresponds to the (1-1-1) plane marked in Figure 2 (a). The HR magnification shown in Figure 3 (e) confirms that the (111) planes exist on both sides of the twin plane. It should be noted that defect-free ZB structure without twin planes was observed at the tip of all investigated NWs before and after the annealing step, as shown in the SI and Figure 2, respectively. Based on these observations, we conclude that type 1 growth is initiated by nucleation of the twin plane which forms the (111)B plane to oppose the initial (1-1-1) plane seen in Figure 2 (a). The two (111)B and (111)A opposing facets pin the droplet to sustain the horizontal growth.

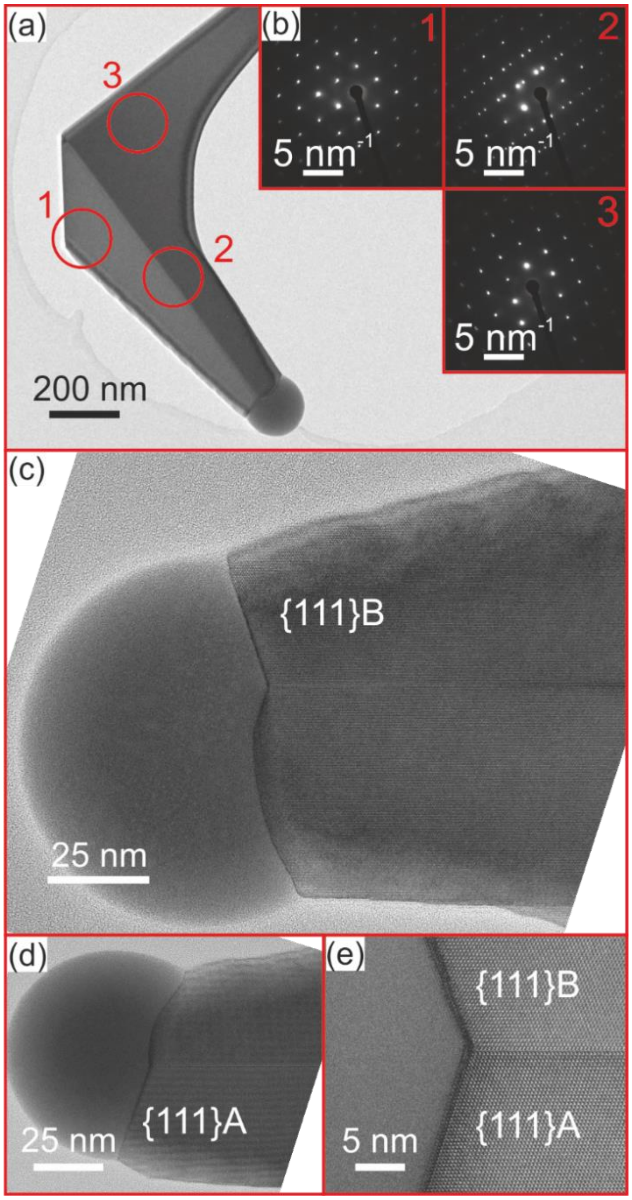

Figure 3. HR-TEM analysis of type 1 bent GaAs NWs. The low magnification image in (a) and selective area diffraction (SAED) patterns in (b) reveal the excellent crystal purity in the ZB phase, and a single twin plane present in the horizontal section. Two different droplet-NW interfaces are dominated by a flat (111)B plane in (c) and (111)A plane in (d). Periodic faceting of the top of the horizontal NW section can clearly be seen in (c) and (d). (e) HR magnification of the twin section that features both (111)A and (111)B facets.

TEM analysis conducted on a type 2 NW structure reveals some similarities with type 1 growth. In particular, Figure 4 (a) shows that type 2 downward growth occurs on a NW where a single twin is present, as we saw earlier for type 1. However, in this case the twin is found in the vertical part, above the downward type 2 growth [Figure 4 (a), SAED pattern 1] and is most likely formed when the growth is resumed. The downward growth continues directly along the <111>B direction [Figure 4 (b)] pointing 109° away from the original NW growth direction. This is the direction of the (-111) facet marked in Figure 2(b). Thus, type 2 downward growth is interpreted to start with nucleation of a single twin plane and the droplet sliding down from the (0-10) facet wetting the (-111) facet marked in Figure 2(b), where the growth continues. During the downward growth, the (-111) facet remains flat and no microfacetting in the droplet-NW interface is witnessed [Figure 4 (b) and SI].

The NW shown in Figure 4 (a) is aligned to a [110] ZA, which is rotated by 60° around the NW axis from the direct side-view [Figure 1(g)]. In this case, possible twinning of the downward part cannot be seen because a twin in that growth direction rotates the zone axis away from the [110]. Hence, only one set of the diffraction points would be seen in the SAED pattern even if the downward section were twinned. Therefore, additional TEM analysis in side-view configuration aligned to [117] ZA is shown in Figure 4 (b), demonstrating that the downward section is dominated by periodic twinning. The twinning is clearly seen as a contrast difference in Figure 4 (b), and is also observable as roughness of the downward section in Figure 4 (a).

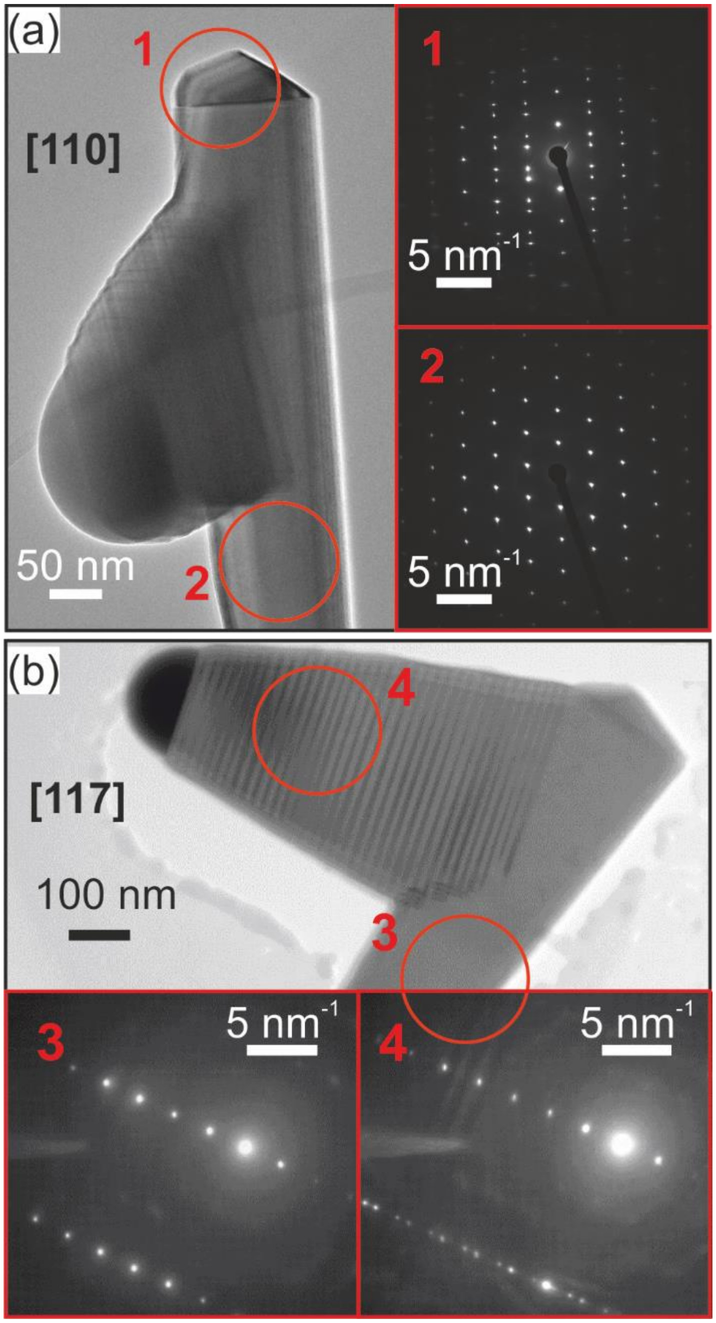

Figure 4. Type 2 downward growth of a GaAs NW. (a) [110] ZA image of a type 2 structure with downward section grown for 20 min shows the defect-free vertical section, with a single twin in the tip of the NW (SAED 1). (b) In [117] ZA image of a structure with 20 min downward growth, periodic twinning of the horizontal section is witnessed, corresponding to SAED 4. The evolution of type 2 structures during the downward growth is described in more detail in the SI.

As type 1 structures grow precisely in the same horizontal plane (see the SI) and exhibit only a single twin plane, whereas type 2 structures consist of a periodic twinning superlattice, we carefully optimized the yield of higher quality type 1 structures. We studied the effects of the NW density, annealing time, V/III BEP ratio during the resumed growth and NW diameter on the populations of type 1 and 2 NWs. For the annealing time, V/III BEP ratio and NW density, all horizontal sections were grown on similar vertical NWs. The effect of each growth parameter was studied independently using the intermediate values of the other two parameters (the NW density = 3×10^7 cm^{-2}, the annealing time = 45 s, the V/III BEP ratio = 9). For the diameter series, the vertical growth time was varied in order to tune the size of the initial NWs (at a fixed V/III BEP ratio). The populations were characterized by analyzing top-view SEM images as described in more detail in the SI.

According to Figure 5 (a), increasing the NW surface density from 2.4×10^7 cm^{-2} to 2.5×10^8 cm^{-2} allowed us to increase the yield of type 1 structures from 20 to 100% . The effect of the annealing time is shown in Figure 5 (b). Very importantly, 99% yield of type 1 structures was obtained with the longest annealing time of 70 s. For the shortest annealing time of 20 s, the horizontal growth was mostly suppressed by the formation of arbitrarily shaped bulges, showing that 20 s is not an adequate time for the deterministic switching of the NW growth direction. Figure 5 (c) shows that altering the V/III ratio as the growth is resumed after the annealing step also had a significant effect on the yield of type 1 structures. For the lowest V/III ratio, all horizontal sections nucleated as type 1 structures. However, for 35% of these structures the droplets wetted the horizontal NW sidewalls, terminating the original type 1 growth. Formation of these structures, referred to as type 1b in the Figure 5 (e), is explained in the SI, where the top facets of such structures are analyzed in more detail based on SEM images. A higher V/III ratio of 11 produced up to 70% yield of type 1 structures. However, many droplets started shrinking during the subsequent horizontal growth, implying that such growth would eventually be terminated due to the droplet consumption. Furthermore, 40% of type 2 structures obtained with V/III=11 exhibited growth directly downward along the sidewalls of vertical NWs. These structures have nucleated similarly to type 2 NWs, and are referred to as type 2b in Figure 5 (e). The SEM analysis of these structures is given in the SI. No droplets were observed on top of type 2b structures.

Figure 5 (d) shows the effect of the NW diameter on the yield of type 1 structures. For the narrowest NWs with the diameters of 75 nm, more than 99% yield of type 1 structures is achieved. Increasing the NW diameter leads to a rapid decrease of the type 1 population. For 84 nm diameter NWs, the type 1 yield becomes only 17.4%, and drops below 10% for 91 nm diameter NWs. The additional data point for 90 nm diameter NWs but with the annealing time increased from 45 s to 70 s demonstrates that type 1 yield increases from less than 10% to 55% despite the large NW diameter. Therefore, increasing the annealing time has a similar effect as decreasing the NW diameter, both leading to higher yield of type 1 structures. This will be important in what follows. Figure 5 (f) shows a SEM image of the high density sample with 100% yield of type 1 NWs.

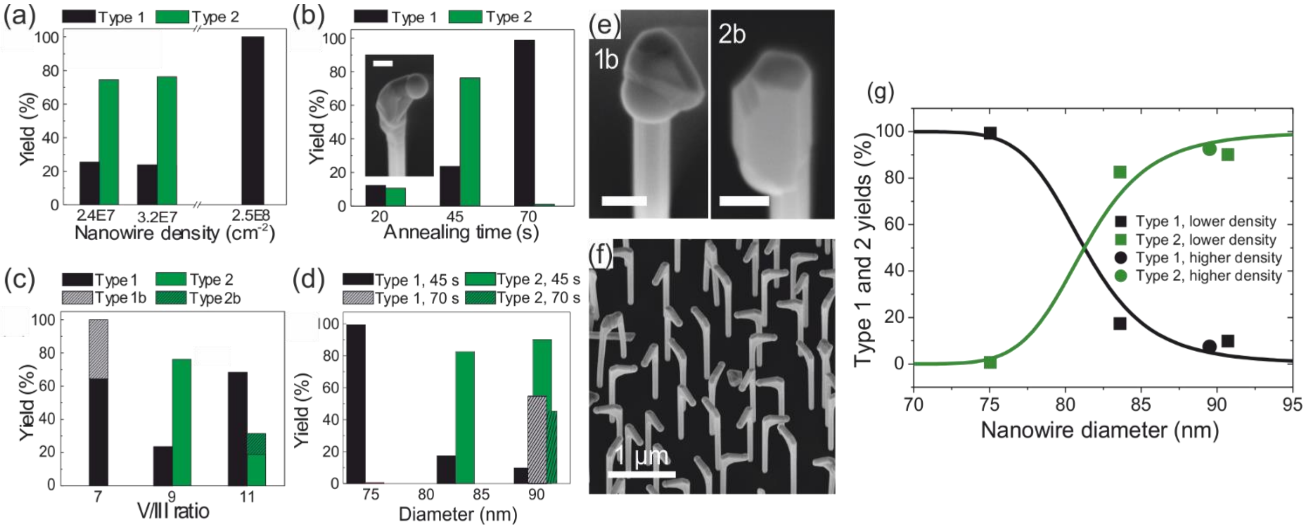

Figure 5. Effect of the growth parameter tuning on the yield of type 1 structures: (a) NW density, (b) annealing time, (c) V/III BEP ratio, and (d) NW diameter. Note that the intermediate data in histograms (a)–(c) are from the same sample. The inset in (b) shows the typical random bulge formed when the annealing time is too short. The 30° tilted view SEM images in (e) show type 1b and 2b structures as described in the text and SI. The scale bars are 100 nm. (f) 30° tilted SEM image of the high density sample with 100% yield of type 1 structures. (g) the NW diameter dependence of the type 1 and 2 populations at a fixed annealing time of 45 s (with a lower density of surface structures of 1.26×10^{8} cm^{-2}, and a higher density of 1.91×10^{8} cm^{-2}), fitted by the model described below.

We now compare these results with the previously published data. The droplet-NW interface reshaping shown in Figure 1 (e) and analyzed in Figure 2 was observed in our previous work [22]. However, as these samples were immediately cooled down after the NW growth, the effect was not reproducible until the annealing step was introduced to achieve the deterministic switching of the NW growth direction as described above. Similar effect of the growth interface reshaping has previously been reported for Be-doped self-catalyzed GaAs NWs in Ref. [27], where Be was thought to lower the droplet surface energy and to cause a partial wetting of the NW sidewalls. In Ref. [28], the Ga flux was provided for 20 to 60 s after termination of the As input in order to inflate the droplet and let it wet the NW side facets. The multiple (111) facets observed in Ref. [27] form a similar structure to the one shown in Figure 2 (a). Similarly in Ref. [28], the (111)A facet dominated the reshaped droplet-NW interface, even though a few twin planes were formed above the droplets, one of which extended to the droplet-NW interface. This extended twin plane is likely to represent the very first steps of nucleation toward type 1 structure. Thus, prior observations support the repeatability and generality of the (111)-dominated droplet-NW interface reshaping upon the growth interruption.

In addition to the reshaped (111)A [(1-1-1) in Figure 2 (a)] facet, our NWs comprise a (100) facet, below which we always observe a (111)B facet [such as the (0-10) and (-111) facets in Figure 2 (b)]. The reshaped (100) facet and the (111)B facet below it were not observed in Refs. [27, 28]. Based on the droplets tilting symmetrically in between the (1-1-1) and (0-10) facets [away from the (-110) NW side facet in Figure 2 (c)], and taking into account the interface configuration observed on the NWs with the droplets removed, we conclude that the reshaped droplet-NW interface consists of a combination of the (111)A and (100) facets, as illustrated in Figure 2 (e)–(h). According to this view, type 1 and type 2 structures nucleate from NWs having very similar droplet-NW interfaces. However, higher quality horizontal type 1 structures are dominated by the (111)A facets. Lower quality downward type 2 structures are dominated by the (100) facets and grow perpendicular to the (111)B facet situated below the (100) one. The difference between type 1 and 2 structures should then be explained by the fine tuning of the interface geometry, namely the probabilities of forming the (111)A and (100) reshaped facets. The reshaping of the growth interface should be due to an interplay of the surface energetics and kinetics, supported by the fact that the populations of type 1 and 2 structures can be tuned by the growth parameters and the NW diameters as shown in Figure 5.

We now present a model to explain and quantify the switching mechanism. According to Refs. [29,30], <111>B-aligned self-catalyzed GaAs NWs and even Au-catalyzed GaAs NWs grown under Ga-rich conditions exhibit a truncated growth interface with an inward tapered facet wetted by a catalyst droplet. Such truncated NWs have pure ZB crystal phase because nucleation occurs away from the triple phase line where solid, liquid and vapor phases meet [29–32]. Unfortunately, *in-situ* TEM measurements [29,31] cannot identify the exact orientation of the small truncated facet due to the complex structure of the truncation and its fast oscillations. However, it seems reasonable that the low index (111)A and (100) can both be present in the initially truncated vertical NWs as well as in NWs reshaping under annealing.

According to the model of Tersoff [31], the free energy change of forming an inclined facet making the angle θ_i to the vertical, of height y and length L, is given by

$$\Delta G_i = L\left[-a_i y + \left(b_i + \frac{\Delta\mu}{\Omega_{35}}\frac{\tan\theta_i}{2}\right)y^2\right]. \tag{1}$$

This expression presents the free energy relative to the vertical facet and planar growth interface. Here, $-a_i$ is the surface energy change upon forming the inclined facet, which becomes negative at large enough contact angles of the droplet β ($\beta \cong 133°$ in our vertical NWs), $\Delta\mu$ is the chemical potential difference per GaAs pair in liquid and solid, $\Omega_{35} = 0.0452$ nm^3 is the elementary volume of GaAs pairs in solid, and b_i is a positive constant which determines the facet size when $\Delta\mu = 0$. The energetically preferred facet heigth $y_*^{(i)}$ that minimizes ΔG_i is given by $y_*^{(i)} = a_i/[2b_i(1+\alpha_i\Delta\mu)]$, with $\alpha_i = \tan\theta_i/(2\Omega_{35}b_i)$. According to our assumption, $a_i > 0$ for both (111)A and (100) facets, with the probability of their occurrence detemining the populations of type 1 ($i=1$) or 2 ($i=2$) bent NW structures. We should now compare the probabilities of forming type 1 or 2 facets at varying chemical potential $\Delta\mu$ which decreases in the annealing stage upon the growth interrupt.

The minimum free energy values at $y = y_*^{(i)}$ are given by

$$\Delta G_*^{(i)} = -\frac{a_i L}{4b_i(1+\alpha_i\Delta\mu)}. \tag{2}$$

The probability p_1 of forming type 1 structure can generally be put as

$$p_1 = \frac{\exp(-\Delta G_1^* / k_B T)}{\exp(-\Delta G_1^* / k_B T) + \exp(-\Delta G_2^* / k_B T)}, \tag{3}$$

with T as the growth temperature and k_B as the Boltzmann constant. As shown in the SI, chemical potential decreases with the annealing time t approximatelly as

$$\Delta\mu = \Delta\mu_0 (1 - \omega t), \quad \omega = \frac{k_B T}{\Delta\mu_0} \frac{3\Omega_3}{\Omega_{35} f(\beta)} k_{35} \frac{h}{R} \propto \frac{1}{R}, \tag{4}$$

with $\Delta\mu_0$ as the initial chemical potential value at $t = 0$. The constant ω determines the rate of chemical potential decrease, with $\Omega_3 = 0.02$ nm^3 as the elementary volume of liquid Ga, $h = 0.326$ nm as the height of GaAs monolayer, $f(\beta) = (1 - \cos\beta)(2 + \cos\beta)/[(1 + \cos\beta)\sin\beta]$ as the geometrical function of the droplet contact angle β, k_{35} as the crystallization rate of GaAs pairs, and R as the NW radius (which equals the radius of the droplet base). Chemical potential decreases linearly with t, while for a given t it is higher for larger R because larger droplets deplete more slowly with their As. Using equations (2) to (4), the yield of type 1 structures is obtained in the form

$$p_1 = \frac{1}{1 + \exp\left[\Gamma\left(\frac{1}{1 + \alpha_2 \Delta\mu_0 (1 - \omega t)} - \frac{u}{1 + \alpha_1 \Delta\mu_0 (1 - \omega t)}\right)\right]}, \tag{5}$$

with $\Gamma = [a_2^2/(4b_2)](L/k_B T)$ and $u = a_1^2 b_2/(a_2^2 b_1)$.

Using the plausible parameters of self-catalyzed growth of GaAs NWs ($\Delta\mu_0 = 0.2$ eV [33,34], k_{35}=165 s^{-1} corresponding to the mean axial growth rate of our vertical NWs of 1.06 nm/s [22], and $\beta = 133^\circ$), we obtain the ω values on the order of 1 min^{-1} for $R \sim$ 50 nm, showing that chemical potential tends to zero after ~ 1 min of annealing. According to Figures 5 (b) and (d), an almost 100% yield of type 1 NW structures is obtained after 70 s annealing and even after 45 s annealing for a smaller NW diameter of 75 nm. Shorter annealing times or larger NW diameters favor type 2 structures, which becomes predominant (more than 90%) for the largest NW diameters of 90–91 nm. According to the above analysis, smaller diameters or longer annealing times bring the VLS system closer to the quasi-equilibrium state at $\Delta\mu = 0$, corresponding to $\omega t = 1$ in equation (5). On the other hand, higher $\Delta\mu$ favors type 2 structures. While the α_i and u parameters entering equation (5) are unknown, higher yield of type 2 structures at $\Delta\mu \cong \Delta\mu_0$ (and therefore the preference of the (100) truncation in vertical NWs), transitioning to an almost 100% yield of type 1 structures at $\Delta\mu \cong 0$ requires that

$$u > 1, \quad \frac{1+\alpha_2\Delta\mu_0}{1+\alpha_1\Delta\mu_0} u < 1, \qquad (6)$$

implying that $\alpha_1 > \alpha_2$. These two inequalities are essential for describing the observed trends in the two competing NW structures under annealing.

Using equation (6), we can quantify the yield of type 1 structures versus the NW diameter at a fixed t of 45 s. The facet length L entering the Γ parameter should be proportional to R. We can then write $\Gamma = R/R_1$ and $\omega t = R_0/R$ according to equation (5). This gives

$$p_1(R) = \frac{1}{1+\exp\left[\frac{R}{R_1}\left(\frac{1}{1+\alpha_2\Delta\mu_0(1-R_0/R)} - \frac{u}{1+\alpha_1\Delta\mu_0(1-R_0/R)}\right)\right]}. \qquad (7)$$

Figure 5 (g) shows a good fit to the data by equation (7) with $R_1 = 1.5$ nm, $R_0 = 32.5$ nm, $u = 2$, $\alpha_2\Delta\mu_0 = 1$ and $\alpha_1\Delta\mu_0 = 7$. It is seen that the transition from less than 10% to almost 100% of type 1 structures is very sharp and occurs for a relatively small diameter change from 90 to 75 nm.

Very importantly, all the statistical data on type 1 versus type 2 NW structures shown in Figures 5 (a) to (d) are qualitatively explained within our model. As discussed above, longer annealing times and smaller NW sizes decrease chemical potential and hence favor type 1 structures. Higher density NWs are ~ 100 nm longer and thinner (71 nm in diameter) than the sparse ones (82 nm in diameter). Therefore, the NW density effect is the same as for the diameter series. Due to a higher fraction of re-emitted As species [33], the local V/III flux ratio should be higher for denser NWs. Higher As flux is known to increase the axial NW growth rate and simultaneously shrink the Ga droplets, yielding thinner NWs [35–37]. Lower V/III BEP ratios leads to a steeper decrease of chemical potential in the gallium droplets [33, 34] and hence favor a faster formation of type 1 structures when the growth is resumed after annealing. The only exception from this trend is the case of the highest V/III BEP ratio of 11 [see Fig. 5 (c)], where the population of type 1 structures increases even though a higher $\Delta\mu$ is expected. This may be associated with shorter incubation times, where more energetically preferred structures are formed over a given period of time. It should also be noted that nucleating the horizontal growth with an optimized V/III BEP ratio for each density (for example, V/III=7 for the intermediate NW density) and then tuning the V/III ratio back to 9 could produce 100% yield of type 1 structures. This gives additional versatility of the growth parameters that can individually be tuned to maximize the deterministic nucleation of type 1 structures.

Based on the structural analysis of the reshaped droplet-NW interfaces and type 1 structures shown in Figures 2 and 3, type 1 structures nucleate on the (1-1-1) facet marked in Figure 2 (a). Simultaneously a twin plane forms, creating a (111)B facet to oppose the (1-1-1) one. Because this twin plane is observed in both types of structures, it is most likely initiated by the triple phase line nucleation at the droplet edge opposing the reshaped (1-1-1) and (0-10) facets, where the droplet contact angle is less than 90° [29, 32]. In type 1 structures, the twin plane between the (111)A and (111)B facets pins the droplet, allowing the growth to propagate in the <112> direction. Such mechanism is known as the twin-mediated growth, observed previously for Ge ingots and Au-catalyzed Ge and GaInP NWs. [38–42] However, our growth mode is different from previous observations. In our case, two different interface configurations are observed, where the flat facet dominating the droplet-NW interface may be either the upper B-polar [Figure 3 (c)], or the lower A-polar facet [Figure 3 (d)], and the other (111) facet is replaced by several smaller microfacets. These two morphologies present different phases of a novel type of twin-mediated growth where the flat facet dominating the growth varies periodically. Oscillations between the flat (111)A and (111)B facets during growth is supported by the periodically changing morphology of the top parts of horizontal NWs, where one half-period is almost parallel to the twin plane and the other has a downward slope with respect to the twin. This fine structure can readily be seen in SEM images shown in Figure 1 (f) and in the SI, and in more detail in the side-view TEM in Figures 3 (c) and (d). The sustainability of this oscillating twin-mediated growth mode for long horizontal sections is demonstrated in the SI by analyzing the horizontal growth rate for a V/III BEP ratio of 9. The growth rate remains constant for at least 20 min and equals the axial-growth rate of vertical NWs (1.06 nm/s).

As regards the surface energetics of horizontal growth, we speculated that the (111)A facets are energetically preferred to all other types of facets at low enough chemical potentials, which is why they are most representative in the reshaped droplet-NW interface. On the other hand, it is known that the (111)B plane of GaAs has a lower energy than the (111)A one (0.69 J/m^2 against 0.82 J/m^2 in contact with As-rich vapors according to Ref. [43]). The same property should pertain when these facets are in contact with the Ga liquid, consistent with the fact that the usual NW growth direction is <111>B [44]. Our type 1 structures nucleate on a (111)A facet, which is inward tapered for vertical NWs and has a lower effective surface energy with respect to the outward tapered (111)B facet [30]. The situation changes after nucleation of a horizontal NW section, where the energetically preferred facet to introduce is the (111)B one, which allows for the stable horizontal growth of type 1 NWs. This explains the unique growth mode whereby the horizontal growth direction is maintained by alternating the (111)A and (111)B facets, and should work equally well for other III-V NWs.

In conclusion, we have demonstrated a high level of control over the growth direction of self-catalyzed GaAs NWs and found a novel type of twin-mediated growth mode, where the growth interface oscillates between the two flat (111) facets with different polarity. By controlling the NW density, annealing time, V/III ratio during the horizontal growth, and the NW diameter, we are able to obtain 100% yield of regular 90° bent NW structures, in which all the horizontal sections start at the pre-determined height. Our model describes an interesting interplay between the surface energetics and growth kinetics, whereby the horizontal growth is preferred at low chemical potentials achieved in the annealing stage. It explains all the observed data and predicts that such morphology should be achievable for any VLS III-V NWs whose growth front is initially truncated. Detailed structural investigations reveal high crystal quality of the obtained structures, which makes them extremely promising for quantum electronic and photonic applications.

ASSOCIATED CONTENT

Supporting Information contains: SEM analysis of NW top faceting; Additional SEM images to support statistical analysis of type 1 and 2 populations; Description of different structures found on the sample; Analysis of horizontal growth rate; Evolution of type 2 downward growth; Additional SEM analysis of growth interface during continued growth; Additional SEM images of exceptions from type 1 and 2 growth due to short annealing or non-optimal V/III BEP ratio; TEM analysis of NWs prior to annealing; Illustrative SEM images of the horizontal plane on which type 1 growth occurs; and Derivation of the chemical potential decrease under annealing.

AUTHOR INFORMATION

Corresponding Author

* Email: eero.koivusalo@tut.fi

Author Contributions

The manuscript was written through contributions of all authors. All authors have given approval to the final version of the manuscript.

ACKNOWLEDGMENT

This work made use of Aalto University Nanomicroscopy Center (Aalto-NMC) and Tampere University of Technology Microscopy center facilities. E.K, T.H and M.G acknowledge financial support from the Academy of Finland projects NESP (decision No. 294630), NanoLight (decision 310985) and the Vilho, Yrjö and Kalle Väisälä Foundation of the Finnish Academy of Science and Letters. H.V.A.G and Y.G.G. acknowledge financial support from São Paulo Research Foundation, FAPESP (decisions grant numbers 14/50513-7 and 16/10668-7). V.G.D. acknowledges the Ministry of Education and Science of the Russian Federation for financial support under grant 14.587.21.0040 (project ID RFMEFI58717X0040).

REFERENCES

[1] B. Mayer, L. Janker, B. Loitsch, J. Treu, T. Kostenbader, S. Lichtmannecker, T. Reichert, S. Morkötter, M. Kaniber, G. Abstreiter, C. Gies, G. Koblmüller, J.J. Finley, Monolithically

Integrated High-β Nanowire Lasers on Silicon, Nano Letters, Vol. 16, Iss. 1, 2016, pp. 152-156, DOI: 10.1021/acs.nanolett.5b03404

[2] K. Tomioka, J. Motohisa, S. Hara, K. Hiruma, T. Fukui, GaAs/AlGaAs Core Multishell Manowire-Based Light-Emitting Diodes on Si, Nano Letters, Vol. 10, Iss. 5, 2010, pp. 1639-1644, DOI: 10.1021/nl9041774

[3] C. Patrik, T. Svensson, T. Mårtensson, J. Trägårdh, C. Larsson, M. Rask, D. Hessman, L. Samuelson, J. Ohlsson, Monolithic GaAs/InGaP nanowire light emitting diodes on silicon, Nanotechnology, Vol. 19, Iss. 30, 2008, pp. 305201, DOI: https://doi.org/10.1088/0957-4484/19/30/305201

[4] J. Wallentin, N. Anttu, D. Asoli, M. Huffman, I. Åberg, M.H. Magnusson, G. Siefer, P. Fuss-Kailuweit, F. Dimroth, B. Witzigmann, H.Q. Xu, L. Samuelson, K. Deppert, M.T. Borgström, InP nanowire array solar cells achieving 13.8% efficiency by exceeding the ray optics limit, Science, Vol. 339, 2013, https://doi.org/10.1126/science.1230969

[5] S. Gazibegovic, D. Car, H. Zhang, S.C. Balk, J.A. Logan, M.W.A. de Moor, M.C. Cassidy, R. Schmits, D. Xu, G. Wang, P. Krogstrup, R.L.M. Op het Veld, K. Zuo, Y. Vos, J. Shen, D. Bouman, B. Shojaei, D. Pennachio, J.S. Lee, P.J. van Veldhoven, S. Koelling, M.A. Verheijen, L.P. Kouwenhoven, C.J. Palmstrøm, E.P.A.M Bakkers, Epitaxy of advanced nanowire quantum devices, Nature, Vol. 548, 2017, pp. 434 , DOI: http://dx.doi.org/10.1038/nature23468

[6] J. Kang, Y. Cohen, Y. Ronen, M. Heiblum, R. Buczko, P. Kacman, R. Popovitz-Biro, H. Shtrikman, Crystal Structure and Transport in Merged InAs Nanowires MBE Grown on (001) InAs, Nano Letters, Vol. 13, Iss. 11, 2013, pp. 5190-5196, DOI: http://dx.doi.org/10.1021/nl402571s

[7] F. Krizek, T. Kanne, D. Razmadze, E. Johnson, J. Nygård, C.M. Marcus, P. Krogstrup, Growth of InAs Wurtzite Nanocrosses from Hexagonal and Cubic Basis, Nano Letters, Vol. 17, Iss. 10, 2017, pp. 6090-6096, DOI: http://dx.doi.org/10.1021/acs.nanolett.7b02604.

[8] T. Rieger, D. Rosenbach, D. Vakulov, S. Heedt, T. Schäpers, D. Grützmacher, M.I. Lepsa, Crystal Phase Transformation in Self-Assembled InAs Nanowire Junctions on Patterned Si Substrates, Nano Letters, Vol. 16, Iss. 3, 2016, pp. 1933-1941, DOI: 10.1021/acs.nanolett.5b05157

[9] D. Dalacu, A. Kam, D.G. Austing, P.J. Poole, Droplet Dynamics in Controlled InAs Nanowire Interconnections, Nano Letters, Vol. 13, Iss. 6, 2013, pp. 2676-2681, DOI: 10.1021/nl400820w

[10] H. Potts, N.P. Morgan, G. Tütüncüoglu, M. Friedl, A. Fontcuberta, i Morral, Tuning growth direction of catalyst-free InAs(Sb) nanowires with indium droplets, Nanotechnology, Vol. 28, Iss. 5, 2017, pp. 054001, DOI: https://doi.org/10.1088/1361-6528/28/5/054001

[11] Y. Luo, C. Chi, M. Jiang, R. Li, S. Zu, Y. Li, Z. Fang, Plasmonic Chiral Nanostructures: Chiroptical Effects and Applications, Advanced Optical Materials, Vol. 5, Iss. 16, 2017, pp. 1700040 DOI: 10.1002/adom.201700040

[12] G. Leahu, E. Petronijevic, A. Belardini, M. Centini, C. Sibilia, T. Hakkarainen, E. Koivusalo, M. Rizzo Piton, S. Suomalainen, M. Guina, Evidence of Optical Circular Dichroism in GaAs-Based Nanowires Partially Covered with Gold, Advanced Optical Materials, Vol. 5, 2017, pp. 1601063, DOI: 10.1002/adom.201601063

[13] E. Petronijevic, M. Centini, A. Belardini, G. Leahu, T. Hakkarainen, C. Sibilia, Chiral near-field manipulation in Au-GaAs hybrid hexagonal nanowires, Optics Express, Vol. 25, Iss. 13, 2017, pp. 14148-14157, DOI: 10.1364/OE.25.014148

[14] A. Kelrich, O. Sorias, Y. Calahorra, Y. Kauffmann, R. Gladstone, S. Cohen, M. Orenstein, D. Ritter, InP Nanoflag Growth from a Nanowire Template by in Situ Catalyst Manipulation, Nano Letters, Vol. 16, Iss. 4, 2016, pp. 2837-2844, DOI: 10.1021/acs.nanolett.6b00648

[15] J. Wang, S. Plissard, M.A. Verheijen, L. Feiner, A. Cavalli, Bakkers, Erik P. A. M., Reversible Switching of InP Nanowire Growth Direction by Catalyst Engineering, Nano Letters, Vol. 13, Iss. 8, 2013, pp. 3802-3806, DOI: 10.1021/nl401767b

[16] S. Conesa-Boj, E. Russo-Averchi, A. Dalmau-Mallorqui, J. Trevino, E.F. Pecora, C. Forestiere, A. Handin, M. Ek, L. Zweifel, L.R. Wallenberg, D. Rüffer, M. Heiss, D. Troadec, L. Dal Negro, P. Caroff, A. Fontcuberta, i Morral, Vertical "III–V" V-Shaped Nanomembranes Epitaxially Grown on a Patterned Si[001] Substrate and Their Enhanced Light Scattering, ACS Nano, Vol. 6, Iss. 12, 2012, pp. 10982-10991, DOI: 10.1021/nn304526k

[17] M. de la Mata, R. Leturcq, S. Plissard, C. Rolland, C. Magén, J. Arbiol, P. Caroff, Twin-Induced InSb Nanosails: A Convenient High Mobility Quantum System, Nano Letters, Vol. 16, Iss. 2, 2016, pp. 825-833, DOI: 10.1021/acs.nanolett.5b05125

[18] F. Lenrick, M. Ek, K. Deppert, L. Samuelson, L.R. Wallenberg, Straight and kinked InAs nanowire growth observed in situ by transmission electron microscopy, Nano Research, Vol. 7, Iss. 8, 2014, pp, DOI: https://doi.org/10.1007/s12274-014-0481-4.

[19] K. Hillerich, K.A. Dick, C. Wen, M.C. Reuter, S. Kodambaka, F.M. Ross, Strategies To Control Morphology in Hybrid Group III–V/Group IV Heterostructure Nanowires, Nano Letters, Vol. 13, Iss. 3, 2013, pp. 903-908, DOI: 10.1021/nl303660h

[20] T.V. Hakkarainen, A. Schramm, J. Mäkelä, P. Laukkanen, M. Guina, Lithography-free oxide patterns as templates for self-catalyzed growth of highly uniform GaAs nanowires on Si(111), Nanotechnology, Vol. 26, 2015, DOI: 10.1088/0957-4484/26/27/275301

[21] E. Koivusalo, T. Hakkarainen, M. Guina, Structural Investigation of Uniform Ensembles of Self-Catalyzed GaAs Nanowires Fabricated by a Lithography-Free Technique, Nanoscale Research Letters, Vol. 12, Iss. 1, 2017, pp. 192, DOI: 10.1186/s11671-017-1989-9

[22] E.S. Koivusalo, T.V. Hakkarainen, M.D. Guina, V.G. Dubrovskii, Sub-Poissonian Narrowing of Length Distributions Realized in Ga-Catalyzed GaAs Nanowires, Nano Letters, Vol. 17, Iss. 9, 2017, pp. 5350-5355, DOI: 10.1021/acs.nanolett.7b01766

[23] C. Colombo, D. Spirkoska, M. Frimmer, G. Abstreiter, A. Fontcuberta, i Morral, Ga-assisted catalyst-free growth mechanism of GaAs nanowires by molecular beam epitaxy, Physical Review B. Vol. 77, 2008, pp. 155326 DOI: 10.1103/PhysRevB.77.155326

[24] E. Uccelli, J. Arbiol, C. Magen, P. Krogstrup, E. Russo-Averchi, M. Heiss, G. Mugny, F. Morier-Genoud, J. Nygård, J.R. Morante, A. Fontcuberta, i Morral, Three-Dimensional Multiple-Order Twinning of Self-Catalyzed GaAs Nanowires on Si Substrates, Nano Letters, Vol. 11, Iss. 9, 2011, pp. 3827-3832, DOI: 10.1021/nl201902w

[25] X. Yuan, P. Caroff, J. Wong-Leung, L. Fu, H.H. Tan, C. Jagadish, Tunable Polarity in a III–V Nanowire by Droplet Wetting and Surface Energy Engineering, Advanced Materials, Vol. 27, Iss. 40, 2015, pp. 6096-6103, DOI: 10.1002/adma.201503540

[26] B. Wacaser, K. Deppert, L. Karlsson, L. Samuelson and W. Seifert, Growth and characterization of defect free GaAs nanowires, Journal of Crystal Growth, Vol. 27, Iss. 2, 2006, pp. 504-508, DOI: //doi.org/10.1016/j.jcrysgro.2005.11.075

[27] Y. Zhang, Z. Sun, A.M. Sanchez, M. Ramsteiner, M. Aagesen, J. Wu, D. Kim, P. Jurczak, S. Huo, L.J. Lauhon, H. Liu, Doping of Self-Catalyzed Nanowires under the Influence of Droplets, Nano Letters, Vol. 18, Iss. 1, 2017, pp. 81-87, DOI: 10.1021/acs.nanolett.7b03366

[28] L. Li, D. Pan, X. Yu, H. So, J. Zhao, Manipulation of morphology and structure of the top of GaAs nanowires grown by molecular-beam epitaxy, Journal of Semiconductors, Vol. 38, Iss. 10, 2017, pp. 103001, DOI: https://doi.org/10.1088/1674-4926/38/10/103001

[29] D. Jacobsson, F. Panciera, J. Tersoff, M.C. Reuter, S. Lehmann, S. Hofmann, K.A. Dick, F.M. Ross, Interface dynamics and crystal phase switching in GaAs nanowires, Nature, Vol. 531, 2016, pp. 317 DOI: http://dx.doi.org/10.1038/nature17148

[30] V.G. Dubrovskii, Development of Growth Theory for Vapor–Liquid–Solid Nanowires: Contact Angle, Truncated Facets, and Crystal Phase, Crystal Growth & Design, Vol. 17, Iss. 5, 2017, pp. 2544-2548, DOI: 10.1021/acs.cgd.7b00076

[31] C.-Y. Wen, J. Tersoff, K. Hillerich, M.C. Reuter, J.H. Park, S. Kodambaka, E.A. Stach, F.M. Ross, Periodically Changing Morphology of the Growth Interface in Si, Ge, and GaP

Nanowires, Physical Review Letters, Vol. 107, Iss. 2, 2011, pp. 025503, DOI: https://doi.org/10.1103/PhysRevLett.107.025503

[32] F. Glas, J. Harmand, G. Patriarche, Why does wurtzite form in nanowires of III-V zinc blende semiconductors? Phys Rev Lett, Vol. 99, Iss. 14, 2007, pp. 146101, DOI: 10.1103/PhysRevLett.99.146101

[33] F. Glas, M.R. Ramdani, G. Patriarche, J. Harmand, Predictive modeling of self-catalyzed III-V nanowire growth, Physical Review B, Vol. 88, Iss. 19, 2013, pp. 195304, DOI: https://doi.org/10.1103/PhysRevB.88.195304

[34] V.G. Dubrovskii, Group V sensitive vapor–liquid–solid growth of Au-catalyzed and self-catalyzed III–V nanowires, in: Journal of Crystal Growth, Vol. 440, Iss. 15, 2016, pp. 62–68, DOI: https://doi.org/10.1016/j.jcrysgro.2016.01.019

[35] T. Rieger, S. Heiderich, S. Lenk, M.I. Lepsa, D. Grützmacher, Ga-assisted MBE growth of GaAs nanowires using thin HSQ layer, Journal of Crystal Growth, Vol. 353, Iss. 1, 2012, pp. 39-46. DOI: https://doi.org/10.1016/j.jcrysgro.2012.05.006

[36] M.R. Ramdani, J.C. Harmand, F. Glas, G. Patriarche, L. Travers, Arsenic Pathways in Self-Catalyzed Growth of GaAs Nanowires, Crystal Growth & Design, Vol. 13, Iss. 1, 2013, pp. 91-96, DOI: 10.1021/cg301167g

[37] M. Federico, V.G. Dubrovskii, D. Rüffer, G. Tütüncüoğlu, Y. Fontana, A. Fontcuberta, i Morral, Tailoring the diameter and density of self-catalyzed GaAs nanowires on silicon, Nanotechnology, Vol. 26, Iss. 10, 2015, pp. 105603, DOI: https://doi.org/10.1088/0957-4484/26/10/105603

[38] E. Billig, Growth of monocrystals of germanium from an undercooled melt, Proceedings of the Royal Society of London.Series A.Mathematical and Physical Sciences, Vol. 229, Iss. 1178, 1955, pp. 346-363, DOI: 10.1098/rspa.1955.0090

[39] D.R. Hamilton, R.G. Seidensticker, Propagation Mechanism of Germanium Dendrites, Journal of Applied Physics, Vol. 31, Iss. 7, 1960, pp. 1165-1168 DOI: 10.1063/1.1735796

[40] A.J. Shahani, P.W. Voorhees, Twin-mediated crystal growth, Journal of Materials Research, Vol. 31, Iss. 19, 2016, pp. 2936-2947, DOI: https://doi.org/10.1557/jmr.2016.308

[41] A.D. Gamalski, P.W. Voorhees, C. Ducati, R. Sharma, S. Hofmann, Twin Plane Re-entrant Mechanism for Catalytic Nanowire Growth, Nano Letters, Vol. 14, Iss. 3, 2014, pp. 1288-1292, DOI: 10.1021/nl404244u

[42] D.S. Oliveira, L.H.G. Tizei, A. Li, T.L. Vasconcelos, C.A. Senna, B.S. Archanjo, D. Ugarte, M.A. Cotta, Interaction between lamellar twinning and catalyst dynamics in spontaneous core–shell InGaP nanowires, Nanoscale, Vol. 7, Iss. 29, 2015, pp. 12722-12727, DOI: 10.1039/C5NR02747K

[43] N. Moll, A. Kley, E. Pehlke, M. Scheffler, GaAs equilibrium crystal shape from first principles, Physical Review B, Vol. 54, Iss. 12, 1996, pp. 8844-8855, DOI: 10.1103/PhysRevB.54.8844

[44] W. Kim, V.G. Dubrovskii, J. Vukajlovic-Plestina, G. Tütüncüoglu, L. Francaviglia, L. Güniat, H. Potts, M. Friedl, J. Leran, A. Fontcuberta i Morral, Bistability of Contact Angle and Its Role in Achieving Quantum-Thin Self-Assisted GaAs nanowires, Nano Letters, Vol. 18, Iss. 1, 2018, pp. 49-57, DOI: 10.1021/acs.nanolett.7b03126.